

Effect of surface stress on Ni segregation in (110) NiAl thin films

J. A. Brown and Y. Mishin

School of Computational Sciences, George Mason University, Fairfax, Virginia 22030, USA

(Received 1 December 2003; published 11 May 2004)

Molecular statics and Monte Carlo simulations in conjunction with an embedded-atom potential are applied to study surface stresses and surface segregation in (110) NiAl free-standing thin films with different thicknesses. Ni always segregates to the surface for both stoichiometric and Ni-rich bulk compositions. The amount of segregation and the lateral deformation of the film both vary in inverse proportion to the film thickness. The size effect of segregation is explained by the elastic deformation of the film in response to the surface stress. It is predicted that the surface free energy decreases and the surface stress increases as the film becomes thinner. These effects are not specific to free-standing films but are also relevant to films on substrates, multilayers, new phase nuclei, and similar situations.

DOI: 10.1103/PhysRevB.69.195407

PACS number(s): 61.43.Bn, 61.50.Nw, 68.35.Ct, 68.47.De

I. INTRODUCTION

Segregation at surfaces and interfaces in alloys and compounds plays a significant role in many processes.^{1,2} In thin films, segregation characteristics may depend on the film thickness for a variety of reasons. One of them is an overlap of opposing near-surface regions affected by the segregation. Another one is the limited amount of the segregating atoms in the film, which leads to a decrease in the bulk concentration as the segregation proceeds.^{3,4} In this paper, we point to yet another possible source of the size effect of segregation. Namely, in a free-standing film, the surfaces produce a homogeneous mechanical stress inside the film.⁵⁻¹⁰ This stress shifts the chemical potentials of atoms in the film and alters the segregation level. The same effect should take place in a film attached to a substrate, except that it is the film/substrate interface stress that gives rise to the bulk stresses.

This effect can only be significant if the film thickness L is small enough to produce a high level of stresses and strains in its interior (bulk). The surfaces of a solid film are always subject to a surface stress τ_{ij} , which is represented by a symmetric tensor with principal values τ_{11} and τ_{22} . Usually both τ_{11} and τ_{22} are positive, meaning that the surfaces are under tension. In an attempt to reduce interatomic distances in the surface layer, the surfaces shrink slightly in an elastic manner and compress the film in lateral directions, thus producing a bulk stress σ_{ij} . For a free-standing film, its dimension normal to the surfaces may increase slightly due to the Poisson effect. Since the surfaces are free, the normal component, σ_{33} , of the bulk stress must be zero. Furthermore, in many cases the principal axes of σ_{ij} in the lateral directions are parallel to the principal axes of τ_{ij} by symmetry. Then, the mechanical equilibrium condition of the film reduces to the simple relations $\sigma_{11} = -2\tau_{11}/L$, $\sigma_{22} = -2\tau_{22}/L$, and $\sigma_{33} = 0$. Introducing the average surface stress $\tau = (\tau_{11} + \tau_{22})/2$ and the hydrostatic bulk pressure $p = -(\sigma_{11} + \sigma_{22} + \sigma_{33})/3$, we have

$$p = \frac{4\tau}{3L}. \quad (1)$$

This equation is a particular case of the more general relation $(3/2)pV = \tau A$, where V and A are the volume and area of the solid.¹¹ It also holds for liquids, except that τ should be replaced by the surface free energy γ . The surface layer of a liquid can contract plastically by burying some of the surface atoms into the bulk, a process in which γ remains constant. In contrast, a solid surface contracts elastically, i.e., without changing the number of atoms exposed to vacuum.

Thus, in a solid film it is important that Eq. (1) includes the surface stress and not the surface free energy. The two quantities are related to one another by^{5,6,10}

$$\tau_{ij} = \delta_{ij}\gamma + \frac{\partial\gamma}{\partial\varepsilon_{ij}}, \quad (2)$$

ε_{ij} being a 2×2 elastic strain tensor of the surface. For the average surface stress we have

$$\tau = \gamma + A \frac{\partial\gamma}{\partial A}. \quad (3)$$

Due to the second term on the right-hand side of this equation, τ can be larger than γ , smaller, or even negative (which γ can never be).

The bulk pressure induced by the surfaces shifts the chemical potential μ_i of each chemical component i by the amount $p v_i$, where v_i is the partial molar volume of the component. Such shifts generally destroy the existing surface-bulk equilibrium and modify the segregations of the components. Furthermore, the accompanying contraction of the film reduces interatomic spacings at the surface and can affect its segregation characteristics as well. The surface free energy may also change as it depends, through the Gibbs adsorption equation, on the chemical potentials, temperature, and the film deformation.⁵ Equation (1) shows that all corrections to thermodynamic quantities arising from the surface stress should decrease with the film thickness as $1/L$.

We will demonstrate this effect by employing a (110) NiAl thin film as a model system. NiAl has a B2 (CsCl-type) structure that accommodates up to 10 at. % deviations from the exact stoichiometry. The choice of NiAl as a model system is dictated by two considerations. First, this compound

has a significant technological importance that motivates a pursuit of fundamental understanding of its physical properties.¹² The surface structure and composition of NiAl are of interest in connection with its oxidation resistance, fracture crack propagation, and other properties.

Secondly, in a previous paper¹³ we have reported atomistic Monte Carlo simulations of the (110), (100), and (111) NiAl surfaces for the stoichiometric and two Ni-rich bulk compositions. The goal of that work was to examine the effect of surface orientation and termination on the surface structure, and in particular to understand the mechanisms by which a NiAl surface can accommodate or eliminate an unfavorable termination. Since we have a well-established methodology for that system, it was advantageous to choose it also for the present work. However, the focus of the present work is essentially different. We now wish to examine the effect of the film thickness on surface segregation and establish the origin of this effect. Thus, in this work we first examine in detail the stress distribution across a (110) NiAl thin film. We then perform accurate Monte Carlo calculations of Ni segregation profiles for several thicknesses of the film and several bulk compositions at a fixed temperature. The results reveal that the segregation isotherm depends on the film thickness. Furthermore, this dependence follows the $1/L$ rule, which proves that the size effect of segregation observed in this work originates from surface stresses.

II. CALCULATION OF SURFACE STRESSES

Atomic interactions in NiAl are modeled by an embedded-atom method (EAM) potential constructed by fitting to experimental and first-principles data.¹⁴ The potential accurately reproduces lattice properties of NiAl, including elastic constants, thermal expansion, and phonon frequencies. It also predicts reasonable values of point-defect energies, planar fault energies, and surface energies, including the reproduction of the rippled relaxation of the (110) surface.¹⁴ This potential was employed in our previous work on NiAl surfaces.¹³

The EAM gives direct access to the mechanical stress tensor on individual atoms. The latter is given by^{15,16}

$$\sigma_{ij}^\alpha = \frac{1}{\Omega_\alpha} \sum_{\beta \neq \alpha} \left[\frac{1}{2} V'_{\alpha\beta}(R_{\alpha\beta}) + F'_\alpha(\bar{\rho}_\alpha) \rho'_\beta(R_{\alpha\beta}) \right] \frac{R_{\alpha\beta i} R_{\alpha\beta j}}{R_{\alpha\beta}}, \quad (4)$$

where the symbols α and β enumerate atoms, i and j are Cartesian components of vectors and tensors, $R_{\alpha\beta}$ is the interatomic distance, $V_{\alpha\beta}(R)$ is the pair interaction function, $\rho_\beta(R)$ is the electron density induced by atom β , $F_\alpha(\bar{\rho})$ is the embedding energy of atom α , $\bar{\rho}_\alpha$ is the background electron density on the location of atom α , and Ω_α is the atomic volume assigned to atom α . While the way the total volume is partitioned between atoms is somewhat arbitrary, the average stress in the solid,

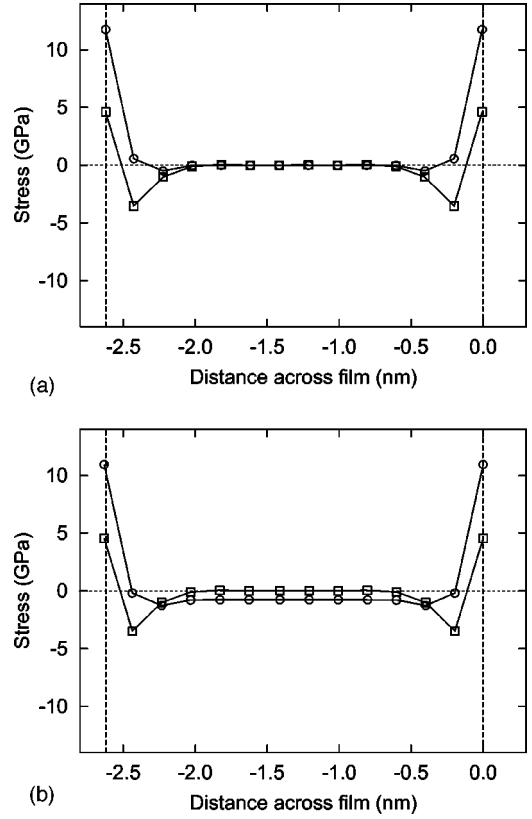


FIG. 1. Calculated lateral (\circ) and normal (\square) mechanical stresses across a (110) NiAl thin film. (a) Unrelaxed state; (b) relaxed state. The vertical dashed lines mark the film surfaces.

$$\bar{\sigma}_{ij} = \frac{1}{V} \sum_{\alpha} \sigma_{ij}^{\alpha} \Omega_{\alpha}, \quad (5)$$

does not depend on the choice of individual atomic volumes. In this work, we choose $\Omega_{\alpha} = \Omega_0$ (equilibrium atomic volume in the perfect lattice).

Figure 1 displays the calculated stress distribution across a 2.6-nm-thick (110) NiAl film. Periodic boundary conditions are applied in directions parallel to the surface. We plot the normal stress σ_{33} and the average lateral stress $\sigma_l = (\sigma_{11} + \sigma_{22})/2$ in individual (110) layers. Each layer contains an equal number of Ni and Al atoms, whose relaxed positions are slightly offset in opposite directions relative to an ideal lattice plane. This so-called rippled relaxation^{17–20} is strongest in the top surface layer and decays rapidly with depth. It should be mentioned that Ni and Al atoms are subject to very different stresses. In the perfect lattice, such stresses are isotropic and equal to -6.38 GPa (compression) for Ni and 6.38 GPa (expansion) for Al, so that the average stress is zero. Near the surface, these stresses become anisotropic and deviate from their bulk values. The stresses plotted in Fig. 1 are averaged over Ni and Al atoms in each (110) layer.

In Fig. 1(a), the film is only relaxed with respect to local atomic displacement while its lateral dimensions are kept fixed at the bulk values. We observe that both σ_{33} and σ_l are zero in the bulk and become positive on the surfaces, reflect-

ing the fact that the surfaces are under tension. One or two under-surface layers, however, are under some compression. For the normal stress σ_{33} , the tension and compression compensate for each other, resulting in the expected relation $\bar{\sigma}_{33}=0$. In contrast, there is a nonzero net lateral stress in the film, $\bar{\sigma}_l$, that allows us to determine the average surface stress τ ,

$$\tau = \frac{L}{2} \bar{\sigma}_l. \quad (6)$$

Calculations from this relation give $\tau=2.40 \text{ J/m}^2$ practically independent of the film thickness. Notice that this surface stress is significantly larger than the surface free energy $\gamma = 1.25 \text{ J/m}^2$ computed with the same EAM potential,¹⁴ suggesting that the term $A \partial \gamma / \partial A$ in Eq. (3) is positive and has the same order of magnitude as γ . A more general form of Eq. (6), $\tau_{ij} = L \bar{\sigma}_{ij} / 2$, allows us to calculate the surface-stress components in the $[1\bar{1}0]$ and $[001]$ directions, $\tau_{[1\bar{1}0]} = 2.90 \text{ J/m}^2$ and $\tau_{[001]} = 1.89 \text{ J/m}^2$. In this work, however, we are only interested in the average stress τ .

In Fig. 1(b), the film is additionally relaxed with respect to *isotropic* deformation in lateral directions. While σ_{33} remains zero, a negative lateral stress appears in the bulk due to a homogeneous elastic deformation of the film under the effect of the surface stress. To test our methodology, Eq. (1) was verified by repeating the calculations for several film thicknesses. In each case, the bulk pressure was computed as $p = -2\bar{\sigma}_{lb}/3$, where $\bar{\sigma}_{lb}$ is the lateral stress averaged over a bulk region undisturbed by the surfaces. In agreement with Eq. (1), a plot of p against $1/L$ was found to follow a straight line whose slope accurately reproduced the result $\tau = 2.40 \text{ J/m}^2$ obtained from Eq. (6).

Alternatively, we can examine the lateral deformation $\varepsilon < 0$ resulting from the film relaxation, which should also follow a linear dependence on $1/L$. Indeed, this deformation is related to $\bar{\sigma}_{lb}$ by $\bar{\sigma}_{lb} = Y\varepsilon$, and therefore $\varepsilon = -(3/2)p/Y$, where Y is the biaxial elastic modulus. In the isotropic approximation, $Y = E/(1-\nu)$, E being the Young modulus and ν Poisson's ratio. Using Eq. (1) we also obtain

$$\varepsilon = -\frac{2\tau}{YL}. \quad (7)$$

Figure 2 verifies that ε obtained by static relaxation is indeed an accurate straight line against $1/L$ provided that $L > 1 \text{ nm}$. It should be mentioned that the normal dimension of the film also experiences deformation by an amount $\varepsilon_{33} > 0$. The latter is proportional to $-\varepsilon$ and, in the isotropic approximation, equals $\varepsilon_{33} = -2\nu\varepsilon/(1-\nu)$. In computations, however, it is easier to measure ε rather than ε_{33} .

As a preparation for the segregation calculations (Sec. III), the effect of thermal expansion was evaluated by *NPT* Monte Carlo simulations. In such simulations, atoms are allowed to move around their lattice positions and the volume can fluctuate by isotropic deformation.^{21,22} The quantity delivered by the simulations is the average lateral deformation ε at a chosen temperature T . Figure 2 shows the deformation

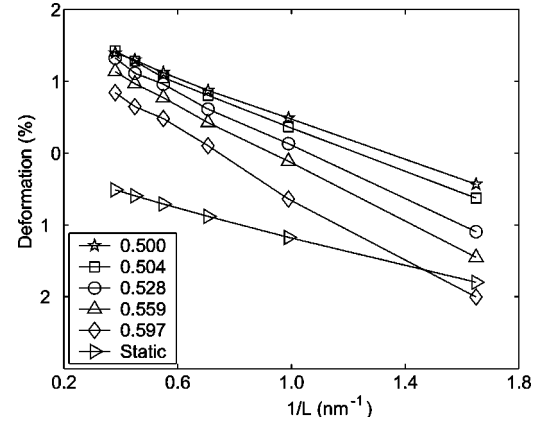


FIG. 2. Lateral deformation of (110) NiAl thin films relative to the bulk state at 0 K as a function of the inverse thickness. Δ , static calculations at 0 K; \star , *NPT* Monte Carlo calculations for stoichiometric composition at 1200 K; all other points, grand-canonical Monte Carlo simulation at 1200 K for nominal bulk compositions indicated in the legend.

computed at $T = 1200 \text{ K}$ for several film thicknesses. As expected, it follows a straight line against $1/L$ ($L > 1 \text{ nm}$). This deformation represents a balance between thermal expansion and elastic contraction in response to the surface stress. When L is small enough, ε becomes negative. On the other hand, as $1/L \rightarrow 0$ it extrapolates to the linear thermal expansion factor of bulk NiAl at this temperature.¹⁴ To a first approximation, thermal expansion simply shifts the line obtained at $T = 0 \text{ K}$ uniformly by the bulk thermal expansion factor. A closer inspection reveals, however, that the Monte Carlo line has a slightly larger slope. According to Eq. (7), this can be caused by either a softening of the material (reduction in Y) or an increase in the surface stress with temperature.

III. MONTE CARLO SIMULATIONS OF SEGREGATION

The surface segregation was studied by Monte Carlo simulations employing the modified grand canonical ensemble in which the temperature, the total number of atoms in the system (N), and the chemical potential difference μ between Ni and Al ($\mu \equiv \mu_{\text{Ni}} - \mu_{\text{Al}}$) are kept fixed whereas the number of atoms of each species can vary.²¹⁻²⁴ The volume of the system is also allowed to fluctuate to simulate zero external pressure conditions. Thus, the system that we simulate contains a constant number of substitutional lattice sites and is connected to an infinite reservoir of heat and Ni and Al atoms. Furthermore, the total number of surface atoms remains fixed, so that the thermal expansion and elastic deformation of the film alter its physical surface area and γ but do so without exposing new atoms to vacuum. In Cahn's terminology,^{5,6} the Lagrangian area A and volume V of the film are fixed while the respective physical quantities can vary. Under such conditions, it is the surface stress τ and not the surface free energy γ that affects the stress state and chemical potentials in the bulk.

At each step of the simulation, an atom is randomly selected and displaced by a relatively small random amount in

TABLE I. Calculated bulk compositions (atomic fraction of Ni) for selected values of the chemical potential difference μ .

| μ (eV) | Composition |
|------------|-------------|
| -1.0 | 0.504 |
| -0.8 | 0.528 |
| -0.7 | 0.559 |
| -0.6 | 0.597 |

an arbitrary direction. Simultaneously, its chemical sort is randomly chosen to either remain unchanged or switch to the alternate species. This trial move is accepted unconditionally if

$$\Delta H \equiv \Delta E \pm \mu \pm \frac{3}{2} k_B T \ln \frac{m_{\text{Ni}}}{m_{\text{Al}}} - N k_B T \ln \frac{V'}{V} < 0 \quad (8)$$

and with the probability of $\exp(-\Delta H/k_B T)$ if $\Delta H > 0$. Here ΔE is the potential energy change in the trial move, V' and V are the new and old volumes, respectively, m_{Ni} and m_{Al} are the atomic masses, and k_B is the Boltzmann constant. The sign in Eq. (8) depends on whether a Ni atom is replaced by Al (+) or vice versa (-). This method allows both compositional rearrangements of atoms and relaxation of their positions to occur simultaneously.

All simulations were implemented at the temperature of 1200 K. Four μ values were chosen, each corresponding to a different equilibrium bulk composition as given in Table I. This correspondence was established by separate simulations performed on a 1024-atom supercell. Throughout this paper, the chemical composition is measured by the atomic fraction of Ni atoms. The bulk compositions include a nearly stoichiometric composition 0.504, two moderately Ni-enriched compositions of 0.528 and 0.559, and a highly Ni-rich composition of 0.597.

The simulation block was brought to equilibrium by 1.5×10^5 Monte Carlo steps per atom followed by 1.5×10^5 more steps for computing the equilibrium distribution of the species. The simulations deliver the average deformation factor (relative to a perfect lattice at 0 K) and the average occupation of every lattice cite. Using such occupations, the Ni concentration profile across the film was calculated by averaging over individual (110) layers each containing 80 atoms. The thickness of the film ranged from four layers (~ 0.6 nm) to 14 layers (~ 2.6 nm).

Figure 3 shows typical concentration profiles obtained for different film thicknesses and bulk compositions. In agreement with our previous work,¹³ the top surface layer is always enriched in Ni while two to three underlayers are depleted in Ni relative to the bulk. The amplitudes of the enrichment and depletion tend to increase as the film thickness decreases. Compositions of deeper layers remain very close to the nominal bulk composition (Table I), except in four- and six-layered films ($L \leq 1$ nm) where the surface regions overlap.

The Gibbsian surface adsorption Γ is an important thermodynamic quantity characterizing the total amount of seg-

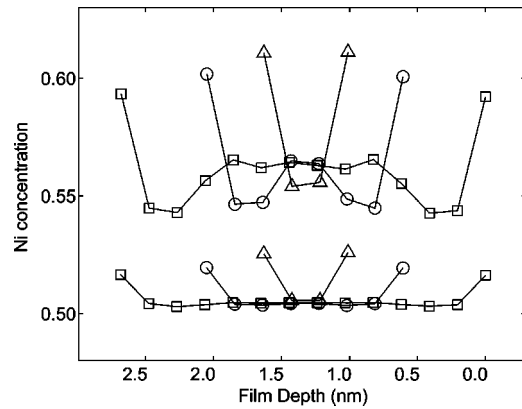


FIG. 3. Calculated composition profiles across the (110) NiAl thin films with selected thicknesses. Obtained by grand canonical Monte Carlo simulations at 1200 K for the nominal bulk compositions of 0.504 (lower plot) and 0.559 (upper plot). The points represent Ni concentrations in individual (110) layers.

regation. It is defined as the number of excess (relative to the bulk) Ni atoms per unit surface area. It was evaluated from the relation

$$\Gamma = \frac{(\bar{c} - c_b)N}{A}, \quad (9)$$

where \bar{c} is the average composition of the simulation block, c_b is the nominal bulk composition (Table I), and A is the total surface area of the film. It is convenient to measure segregation by the effective number of monolayers (ML). This number is found by dividing Γ obtained from Eq. (9) by the number of atoms per unit area of a (110) plane. It should be pointed out that the use of the nominal bulk composition instead of the actual one is only justified when the film is sufficiently thick (six layers or more, or $L > 1$ nm).

In Fig. 4, the Gibbsian adsorption is plotted against $1/L$ for different bulk compositions. The important observation is that Γ is approximately a linear function of $1/L$. The scatter of the points for the Ni-rich bulk (0.597) is due to the for-

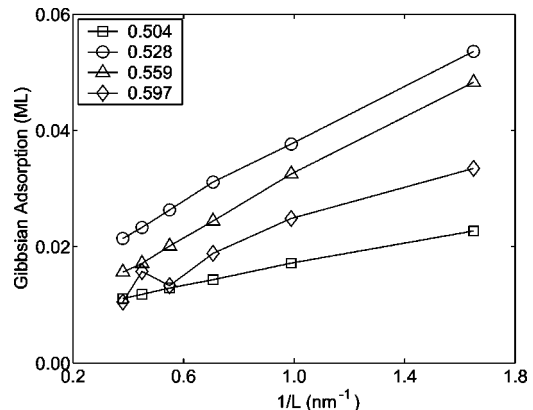


FIG. 4. Calculated Gibbsian adsorption in (110) NiAl thin films as a function of the inverse film thickness for nominal bulk compositions indicated in the legend. Obtained by grand canonical Monte Carlo simulations at 1200 K.

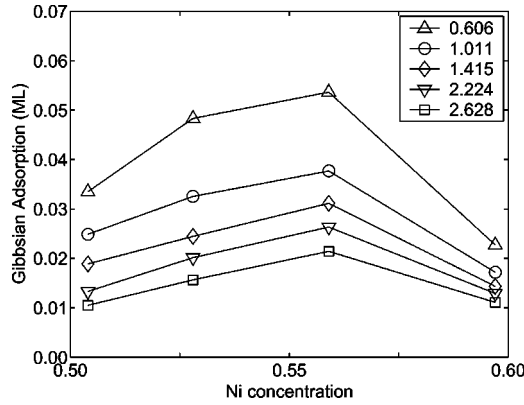


FIG. 5. Isotherms of Ni segregation in (110) NiAl thin films at 1200 K. The film thicknesses (in nm) are indicated in the legend.

mation of isolated Ni Frenkel pairs (Ni vacancy plus Ni adatom) on the surface during the simulations. Such pairs, which were only observed for this bulk composition, distort the concentration profile and have a significant effect on Γ .

Finally, Fig. 5 displays isotherms of Ni segregation (Γ versus bulk composition) for selected film thicknesses. For bulk compositions exceeding 0.56, the isotherm becomes essentially nonlinear, with downward deviations indicative of a saturation effect. Although the segregation itself is relatively small in this material, it can be enhanced by the size effect up to a factor of 2.

IV. DISCUSSION AND CONCLUSIONS

Returning to Fig. 2, the Monte Carlo simulations reveal that the lateral deformation ε of the film varies in inverse proportion to its thickness and that the bulk off-stoichiometry towards Ni gradually shifts the ε versus $1/L$ line towards smaller deformations. The latter is understandable since Ni has a considerably smaller atomic size than Al and reduces the equilibrium lattice parameter of the alloy. Perhaps more interestingly, the slope of the line tends to increase slightly with Ni bulk concentration, the likely reasons being either a softening of the material (decrease of the biaxial modulus) or an increase in the surface stress [cf. Eq. (7)].

In a closed system, the bulk pressure p would shift the chemical potential difference μ by the amount of pv , where $v = v_{\text{Ni}} - v_{\text{Al}} < 0$ is the difference between the molar volumes of Ni and Al.²⁶ Since our Monte Carlo simulations kept μ fixed (open system), the bulk composition was expected to alter by an amount δc that would balance the pressure-related shift in μ . The balance condition reads

$$\left(\frac{\partial \mu}{\partial c}\right)_{p,T} \delta c + pv = 0. \quad (10)$$

We notice from Table I that $(\partial \mu / \partial c)_{p,T} > 0$. Given that $p > 0$ and $v < 0$, δc must be positive. We could not detect any changes in the bulk composition with L within the accuracy of our simulations. Although longer Monte Carlo runs could have revealed such changes, they are clearly very small. This is not surprising considering that NiAl is a highly ordered compound with a strong tendency to maintain its stoichiom-

etry. Noticeable changes in the bulk composition would probably require greater pressures than those developed in our films.

For the same reason, Ni segregation remains quite small regardless of the film thickness. Yet it does show a clear trend to increase as L decreases (Fig. 4). This increase could not be caused by an overlap of the surface regions (films with $L > 1$ nm are too thick for that) or changes in the bulk composition (as stated above, it did not practically change). At the same time, both the segregation and the accompanying lateral deformation of the film show a linear dependence on $1/L$ characteristic of surface-induced stresses (Figs. 2 and 4). This observation firmly validates that the size effect of surface segregation observed in our films is caused by surface stresses. On the atomic level, the dominant factor responsible for this effect is likely to be the contraction of interatomic distances in the surface region due to the lateral deformation of the film. This contraction is accommodated by an adsorption of an additional amount of relatively small Ni atoms.

Some further trends can be predicted from thermodynamic considerations. If we fix the temperature and the film dimensions, the Gibbs adsorption equation reduces to $d\gamma = -\Gamma d\mu$.^{5,25} Since $\Gamma > 0$ (Fig. 4), it follows that the surface free energy should decrease with μ . Remembering that the bulk concentration increases with μ (Table I), we conclude that deviations from stoichiometry towards Ni should lower γ .

Now suppose T and μ are fixed (grand-canonical ensemble) while the lateral deformation ε varies in response to variations in L . The relevant change in γ is represented by the second term in Eq. (3), which can be rewritten as $(1/2)\partial\gamma/\partial\varepsilon$. The factor 1/2 comes from the relation $dA = 2Ad\varepsilon$ that reflects the 2D nature of the surface. As we established by static calculations at 0 K, this term is positive and relatively large (1.16 J/m^2 , see Sec. II). Assuming that it remains positive at elevated temperatures and recalling that ε and L are related through Eq. (7), we use the chain rule to obtain

$$\frac{\partial \gamma}{\partial \varepsilon} = \frac{\partial \gamma}{\partial L} \frac{\partial L}{\partial \varepsilon} = \frac{YL^2}{2\tau} \frac{\partial \gamma}{\partial L} > 0.$$

Because $Y > 0$ and $\tau > 0$, we can conclude that γ increases with L . In other words, the surface free energy decreases as the film becomes thinner.

Since Ni atoms are relatively small, Ni segregation can be expected to decrease the equilibrium lattice spacing at the surface and thus increase the surface stress (recall that the surface region is under tension relative to the equilibrium lattice spacing at the surface). As the film becomes thinner and the segregation level increases, so does the surface stress. Figure 4 suggests that this effect can be further amplified by deviations from bulk stoichiometry towards Ni, since such deviations favor Ni segregation. This can explain the increase in the slopes of the ε versus $1/L$ lines with off-stoichiometry observed in Fig. 2. Overall, the surface

free energy in (110) NiAl thin films is lower while the surface stress is higher than in thick samples with the same surface orientation.

Although we believe that the EAM potential used in this work is accurate, some of the numbers reported here can be specific to this potential. However, the general trends discussed here must be the same, as they reflect basic thermodynamics and should not depend on specific details of atomic interactions.

It should be emphasized that we have analyzed a free-standing thin film only as a simple model suitable for demonstrating the physical effect (impact of surface stress on segregation). Experimental measurements on free-standing thin films are highly problematic.^{7,9} However, this effect is equally relevant to a film on a substrate, multilayers (superlattices), early stages of depositions, epitaxy, and many other situations involving interface stresses. It can also influence the nucleation of a second phase precipitating in a matrix or

at interfaces. It should also be mentioned that grain boundary segregation in nanostructured materials can be subject to the size effect caused by grain boundary stresses.

Likewise, NiAl was only used here as a model material. In fact, due to its strong ordering tendency and low segregation level, this material probably underestimates the strength of the effect. In the future, it would be interesting to examine the size dependence of surface and interface segregation in disordered alloys.

ACKNOWLEDGMENTS

We are grateful to A. Suzuki for help with some of the calculations and to A. Y. Lozovoi for carefully reading the manuscript and making useful points. This work was supported by the U.S. Department of Energy (Office of Basic Energy Sciences) under Grant No. DE-FG02-01ER4545871.

¹A.P. Sutton and R.W. Balluffi, *Interfaces in Crystalline Materials* (Clarendon Press, Oxford, 1995).

²*Materials Interfaces: Atomic-level Structure and Properties*, edited by D. Wolf and S. Yip (Chapman & Hill, London, 1992).

³C. Cserhati, I.A. Szabo, and D.L. Beke, *J. Appl. Phys.* **83**, 3021 (1998).

⁴A.V. Krajinikov, V.M. Yurchenko, E.P. Feldman, and D.B. Williams, *Surf. Sci.* **515**, 36 (2002).

⁵J.W. Cahn, *Thermodynamics of Solid and Fluid Surfaces*, in *Interface Segregation*, edited by W.C. Johnson and J.M. Blackely (American Society of Metals, Metals Park, OH, 1979), Chap. 1, p. 3.

⁶J.W. Cahn, *Acta Metall.* **28**, 1333 (1980).

⁷R.C. Cammarata, *Prog. Surf. Sci.* **46**, 1 (1994).

⁸W.D. Nix and H. Gao, *Scr. Mater.* **39**, 1653 (1998).

⁹F. Spaepen, *Acta Mater.* **48**, 31 (2000).

¹⁰C. Herring, *The Use of Classical Macroscopic Concepts in Surface-energy Problems*, in *Structure and Properties of Solid Surfaces*, edited by R. Gomer and C.S. Smith (University of Chicago Press, Chicago, 1953), Chap. 1, pp. 5–81.

¹¹J. Weissmuller and J.W. Cahn, *Acta Mater.* **45**, 1899 (1997).

¹²*Intermetallic Compounds: Structural Applications*, edited by J.H. Westbrook and R.L. Fleischer (Wiley & Sons, New York, 2000),

Vol. 4.

¹³J.A. Brown and Y. Mishin, *Phys. Rev. B* **67**, 195414 (2003).

¹⁴Y. Mishin, M.J. Mehl, and D.A. Papaconstantopoulos, *Phys. Rev. B* **65**, 224114 (2002).

¹⁵G.J. Ackland and M.W. Finnis, *Philos. Mag. A* **54**, 301 (1986).

¹⁶P. Gumbsch and M.S. Daw, *Phys. Rev. B* **44**, 3934 (1991).

¹⁷H.L. Davis and J.R. Noonan, *Phys. Rev. Lett.* **54**, 566 (1985).

¹⁸M.H. Kang and E.J. Mele, *Phys. Rev. B* **36**, 7371 (1987).

¹⁹S.P. Chen, A.F. Voter, and D.J. Srolovitz, *Phys. Rev. Lett.* **57**, 1308 (1986).

²⁰S.P. Chen, A.F. Voter, and R.C. Albers, *Phys. Rev. B* **39**, 1395 (1989).

²¹S.M. Foiles, *Phys. Rev. B* **32**, 7685 (1985).

²²D. Frenkel and B. Smit, *Understanding Molecular Simulation* (Academic Press, San Diego, 2002).

²³S.M. Foiles and M.S. Daw, *J. Mater. Res.* **2**, 5 (1987).

²⁴S.M. Foiles, *Calculation of the Surface Segregation of Alloys Using the Embedded Atomic Method*, in *Surface Segregation Phenomena*, edited by P. Dowben and A. Miller (CRC Press, Boca Raton, FL, 1990), p. 79.

²⁵M.W. Finnis, *Phys. Status Solidi A* **166**, 397 (1998).

²⁶Simple numerical estimates show that under our simulation conditions, pv is on the order of 0.01 eV.